JACS
JOURNAL OF THE AMERICAN CHEMICAL SOCIETY
Article
pubs.acs.org/JACS

From 1D Chain to 3D Network: A New Family of Inorganic–Organic Hybrid Semiconductors $MO_3(L)_x$ (M = Mo, W; L = Organic Linker) Built on Perovskite-like Structure Modules

Xiao Zhang,[†] Mehdi Hejazi,[‡] Suraj J. Thiagarajan,[§] William R. Woerner,[∥] Debasis Banerjee,[†] Thomas J. Emge,[†] Wenqian Xu,[⊥] Simon J. Teat,[#] Qihan Gong,[†] Ahmad Safari,[‡] Ronggui Yang,[§] John B. Parise,[∥] and Jing Li*[,†]

[†]Department of Chemistry and Chemical Biology, Rutgers University, 610 Taylor Road, Piscataway, New Jersey 08854, United States
[‡]Department of Material Science and Engineering, Rutgers University, 607 Taylor Road, Piscataway, New Jersey 08854, United States
[§]Department of Mechanical Engineering, University of Colorado, 111 Engineering Drive, Boulder, Colorado 80309, United States
[∥]Department of Geosciences, Stony Brook University, 255 Earth and Space Sciences Building, Stony Brook, New York 11794, United States
[⊥]Chemistry Department, Brookhaven National Laboratory, P.O. Box 5000, Upton, New York 11973, United States
[#]Advanced Light Source, Lawrence Berkeley National Laboratory, 6 Cyclotron Road, Berkeley, California 94720, United States

Supporting Information

ABSTRACT: MO_3 (M = Mo, W) or VI–VI binary compounds are important semiconducting oxides that show great promise for a variety of applications. In an effort to tune and enhance their properties in a systematic manner we have applied a designing strategy to deliberately introduce organic linker molecules in these perovskite-like crystal lattices. This approach has led to a wealth of new hybrid structures built on one-dimensional (1D) and two-dimensional (2D) VI–VI modules. The hybrid semiconductors exhibit a number of greatly improved properties and new functionality, including broad band gap tunability, negative thermal expansion, largely reduced thermal conductivity, and significantly enhanced dielectric constant compared to their MO_3 parent phases.

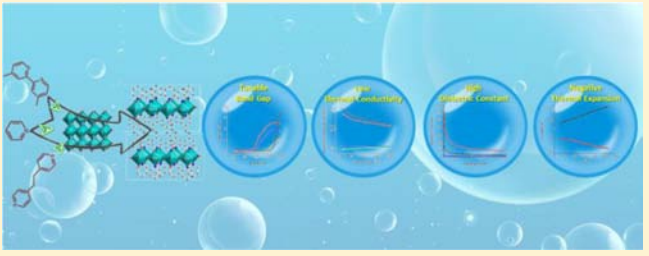

INTRODUCTION

In addition to their structural rigidity and stability, excellent electronic, optical, magnetic, and transport properties of inorganic materials make them highly attractive for practical applications. On the other hand, organic compounds built on simple molecules are well-known for their flexibility, easy processability, synthesis controllability, and relatively low cost. Incorporation and integration of the two counterparts into a single crystal lattice may yield inorganic–organic hybrid crystalline materials that possess not only combined or enhanced properties of the individual components, but also new phenomena and unprecedented features not possible with either component alone.[1−8] Over the past decade, great efforts have been made in developing new types of hybrid materials and exploring their unique functionalities. These include structures in which organic and inorganic component are connected via ionic bonding[9,10] or relatively weak H-bonding and van der Waals interactions,[11−14] as well as those constructed on covalently bonded inorganic and organic nanomodules.[8] One family of the latter group is the II–VI based hybrid semiconductors[15−19] with a general formula of $[MQ(L)_x]$ (M = Mn, Zn, Cd; Q = S, Se, Te; L = mono- or diamine, x = 0.5 or 1). These crystalline compounds are extended networks of 1D, 2D, and 3D and are composed of alternating II–VI binary semiconductor (inorganic component) modules and acyclic amines (organic component) at nano- or subnanometer scale via coordinate bonds. They exhibit a number of enhanced properties over their parent II–VI semiconductors, as well as new phenomena. These include strong structure-induced quantum confinement effect (QCE), high absorption power, direct white light emission, anisotropic zero thermal expansion, and temperature-dependent phase transitions, to name a few.[18,20−28] In addition, low-cost and simple one-pot synthesis, solution processability and ease for scale-up, well-defined and precisely controlled crystal structures and composition, as well as good thermal stability (up to 200 °C), are all attractive features that make them promising candidates for various applications.

Inspired by the success in II–VI based hybrid semiconductors, we have looked into the possibility of assembling hybrid structures built on other important semiconductors,

Received: August 1, 2013
Published: October 23, 2013

   dx.doi.org/10.1021/ja4077556 | J. Am. Chem. Soc. 2013, 135, 17401−17407

such as metal oxides. The binary MoO_3 and WO_3 have been extensively studied for possible applications in solar energy conversion.[29,30] For example, WO_3 has been well investigated for its use in photochemical water oxidation and dye-sensitized solar cells. Much effort is currently being made to tune its band gap and Fermi energy.[31−33] Interestingly both MoO_3 and WO_3 are also considered for applications in lithium ion battery anodes and electrochromic windows.[34,35] Furthermore, studies have shown that MoO_3 may be a suitable component for composite thermoelectric devices.[36] Hybrid semiconductors based on MO_3 (M = Mo, W) are likely to have greatly enhanced properties and new functionality, as found in the II−VI hybrid structures. Here we report the design, synthesis, and unique properties of a hybrid semiconductor family $MO_3(L)$ (L = organic linker) composed of periodically ordered 1D and 2D perovskite-like modules of MO_3 (see Table 1).

EXPERIMENTAL SECTION

Materials and Instruments. Materials used include MoO_3 (99.5%, Merck), $3Na_2WO_4{\cdot}9WO_3{\cdot}H_2O$ (>98%, Alfa Aesar), pyrazine (>99%, Research Chemicals Ltd.), 4,4′-bipyridine (98%, Alfa Aesar), 1,2-di-(4-bipyridyl)ethane (99%, Aldrich), 1,2-di-(4-bipyridyl)ethylene (97%, Aldrich), pyridine (99%, Aldrich), 4,4-dimethyl-2,2-bipyridine (99%, Alfa Aesar), Bi_2O_3 (99%, Alfa Aesar), WO_3 (99%, Fisher Scientific), and tungsten powder (99.9%, Strem Chemicals). Reactions were carried out either in sealed thick-wall Pyrex tubes (2.5 mL) or sealed acid digestion bombs (23 mL).

Table 1. List of $MO_3(L)$ Compounds[37−39] with Their Unit Cell Parameters, Space Groups (SGs), and Experimental Optical Band Gaps (BGs)

compd[a]	unit cell constants (Å, deg)	space group	band gap (eV)
1D-MoO_3(4,4′-dm-2,2′-bpy) (**1**)	a = 3.7772(7)	$P2_1/c$	3.3
	b = 15.242(3)		
	c = 20.400(4)		
	β = 95.296(4)		
1D-WO_3(4,4′-dm-2,2′-bpy) (**2**)	a = 3.7218(2)	$P2_1/c$	3.2
	b = 15.3615(2)		
	c = 20.3617(8)		
	β = 94.816(6)		
2D-MoO_3(py) (**3**)	a = 7.5228(4)	$Pbca$	2.4
	b = 7.3890(4)		
	c = 22.6080(13)		
2D-WO_3(py) (**4**)	a = 7.5024(0)	$Pbca$	2.35
	b = 7.4283(1)		
	c = 22.9359(2)		
3D-$MoO_3(pyz)_{0.5}$ (**5**)	a = 5.2702(15)	$I222$	2.3
	b = 5.2674(7)		
	c = 14.2310(11)		
3D-$WO_3(pyz)_{0.5}$ (**6**)	a = 5.2288(7)	$I4/mmm$	2.2
	b = 5.2288(7)		
	c = 14.175(3)		
3D-$MoO_3(4,4'\text{-bpy})_{0.5}$ (**7**)	a = 7.5727(6)	$P2_1/c$	2.3
	b = 7.3675(7)		
	c = 22.433(3)		
	β = 90.396(8)		
3D-$WO_3(4,4'\text{-bpy})_{0.5}$ (**8**)	a = 7.4733(15)	$Cmca$	2.25
	b = 7.3927(15)		
	c = 22.570(4)		
3D-$WO_3(bpe)_{0.5}$ (**9**)	a = 5.2546(3)	$I\bar{4}2m$	2.3
	b = 5.2546(3)		
	c = 26.987(3)		

[a]4,4′-dm-2,2′-bpy = 4,4′-dimethyl-2,2′-bipyridine, py = pyridine, pyz = pyrazine, 4,4′-bpy = 4,4′-bipyridine, bpe = 1,2-bipyridylethane.

Synthesis of $MoO_3(L)$ Inorganic−Organic Hybrid Materials. *Synthesis of [1D-MoO_3(4,4′-dm-2,2-bpy)] (4,4′-dm-2,2-bpy = 4,4-Dimethyl-2,2-bipyridine) (**1**).* Reactions of MoO_3 (0.036 g, 0.25 mmol, 0.25 M) and 4,4-dimethyl-2,2-bipyridine (0.080 g, 0.43 mmol, 0.43 M) in water (1 mL) in a thick-wall Pyrex tube at 150 °C for 5 days afforded colorless crystals (75.4% yield based on Mo) of **1** were collected after filtration.

*Synthesis of [1D-WO_3(4,4′-dm-2,2-bpy)] (4,4′-dm-2,2-bpy = 4,4-Dimethyl-2,2-bipyridine) (**2**).* The compound was synthesized by reacting $3Na_2WO_4{\cdot}9WO_3{\cdot}H_2O$ (0.036 g, 0.12 mmol, 0.12 M) with 4,4-dimethyl-2,2-bipyridine (0.080 g, 0.43 mmol, 0.43 M) in water (1 mL) at 150 °C for 5 days in a thick-wall Pyrex tube. $3Na_2WO_4{\cdot}9WO_3{\cdot}H_2O$ served as W metal source in both WO_3 and WO_4^{2-} form which were required to produce the desired hybrid compound **2**. Colorless crystals of **2** (73.2% yield based on W) were isolated after filtration.

*Synthesis of [2D-MoO_3(py)] (py = Pyridine) (**3**).* A reaction of MoO_3 (0.15 g, 1.04 mmol, 2.08 M) and pyridine (0.5 mL, 6.25 mmol) at 150 °C for 20 days in thick-wall Pyrex tube produced yellow plate-like crystals of **3**. The product was washed by ethanol, water, and anhydrous ethyl ether in sequence (yield ca. 80% based on MoO_3).

*Synthesis of [2D-WO_3(py)] (py = Pyridine) (**4**).* A stoichiometric mixture of Bi_2O_3 (4.659 g, 10 mmol) and WO_3 (4.637 g, 20 mmol) was calcined at 800 °C for 48 h to synthesize $Bi_2W_2O_9$. The product was stirred in 1 M hydrochloric acid for 5 days to generate pure $H_2W_2O_7{\cdot}xH_2O$. The as-formed $H_2W_2O_7{\cdot}xH_2O$ (0.1 g, ∼0.2 mmol, 0.4 M) was then reacted with pyridine (0.5 mL, 6.25 mmol) at 150 °C for 10 days in thick-wall Pyrex tube to yield yellow powders of **4**. The product was washed by ethanol, water, and anhydrous ethyl ether in sequence (ca. 70% yield based on tungsten).

*Synthesis of [3D-$MoO_3(pyz)_{0.5}$] (pyz = Pyrazine) (**5**).* Compound **5** was prepared from the reactions of MoO_3 (0.16 g, 1.1 mmol, 0.11 M), $CuCl_2{\cdot}2H_2O$ (0.11 g, 0.64 mmol, 0.064 M), pyrazine (0.23 g, 2.9 mmol, 0.29 M), and 10 mL of H_2O in a 23 mL acid digestion bomb at 160 °C for 5 days. The presence of $CuCl_2{\cdot}2H_2O$ was crucial for generating a pure product.[37] The dark blue powders were washed with water and 95% ethanol and then heated in the air at 150 °C for 12 h. The orange powder of **5** was collected in 50% yield based on MoO_3.

*Preparation of [3D-$WO_3(pyz)_{0.5}$] (pyz = Pyrazine) (**6**).* Compound **6** was synthesized from the reactions of W (0.072 g, 0.39 mmol, 0.049 M), $3Na_2WO_4{\cdot}9WO_3{\cdot}H_2O$ (0.36 g, 0.12 mmol, 0.015 M), pyrazine (0.072 g, 0.9 mmol, 0.011 M), and 8 mL of H_2O in a 23 mL acid digestion bomb at 150 °C for 7 days. The use of W metal was crucial for the formation of compound **6**.[38] After systematic cooling at the speed of 0.1 °C/min to room temperature, dark blue black crystals of **6** were collected by vacuum filtration and dried (yield ca. 50% based on $3Na_2WO_4{\cdot}9WO_3{\cdot}H_2O$).

*Synthesis of [3D-$MoO_3(4,4'\text{-bpy})_{0.5}$][39] (4,4-bpy = 4,4′-Bipyridine) (**7**).* Compound **7** was obtained from reactions of MoO_3 (0.152 g, 1.06 mmol, 0.177 M), 4,4′-bipyridine (0.144 g, 0.92 mmol, 0.153 M), and H_2O (6 mL) in a 23 mL acid digestion bomb at 150 °C for 5 days. The product was washed by 30% ethanol and water, followed by drying in anhydrous ethyl ether. The orange crystals of **7** were isolated (highest yield ∼70% based on MoO_3).

*Preparation of [3D-$WO_3(4,4\text{-bpy})_{0.5}$][38] (4,4-bpy = 4,4-Bipyridine) (**8**).* A mixture of 4,4′-bipyridine (0.144 g, 0.92 mmol, 0.115 M), $3Na_2WO_4{\cdot}9WO_3{\cdot}H_2O$ (0.45 g, 0.15 mmol, 0.019 M), and H_2O (8 mL) was placed in a 23 mL acid digestion bomb, and the Teflon-lined Parr acid digestion bomb was heated for 7 days at 150 °C under autogenous pressure. After allowing the reaction mixture to cool to room temperature, yellow crystal plates of **8** were collected by filtration and dried at room temperature (yield ca. 70% based on WO_3).

*Synthesis of [3D-$WO_3(bpe)_{0.5}{\cdot}0.14\ H_2O$] (bpe = 1,2-Di-(4-bypiridyl)ethane) (**9**).* Compound **9** was prepared from the reactions of W (0.072 g, 0.39 mmol, 0.0488 M), $3Na_2WO_4{\cdot}9WO_3{\cdot}H_2O$ (0.36 g, 0.12 mmol, 0.015 M), 1,2-di-(4-bypiridyl)ethane (0.072 g, 0.39 mmol,

dx.doi.org/10.1021/ja4077556 | J. Am. Chem. Soc. 2013, 135, 17401−17407

0.049 M), plus H_2O (8 mL) in a 23 mL acid digestion bomb at 150 °C for 7 days. The dark blue crystals were washed with water and 95% ethanol and then heated in the air at 150 °C for 12 h. The yellow crystals of **9** were collected (yield ca. 40% based on W).

Cold-Pressing of Pellets. Circular pellets were made by loading the powder in a circular die (12.8 mm diameter) and pressed at different pressures for 4 h in a Carver laboratory press, followed by annealing at various temperatures for 24 h.

Diffuse Reflectance Measurements. Optical diffuse reflectance spectra were measured at room temperature with a Shimadzu UV-3101PC double beam, double monochromator spectrophotometer. Data were collected in the wavelength range 250−2000 nm. $BaSO_4$ powder was used as a standard (100% reflectance). A similar procedure as previously described was used to collect and convert the data using the Kubelka−Munk function. The scattering coefficient (S) was treated as a constant since the average particle size of the samples used in the measurements was significantly larger than 5 nm.

Thermogravimetric (TG) Analysis. TG analyses of the title compounds were performed on a computer-controlled TG Q50 analyzer (TA Instrument). Single-phased powder samples were loaded into platinum pans and heated with a ramp rate of 10 °C/min from room temperature to 600 °C.

Single Crystal X-ray Diffraction (SXRD). Single crystal X-ray diffraction data of the compounds were collected at low temperature (100 K) on a Bruker-AXS smart APEX I CCD diffractometer with graphite-monochromated Mo Kα radiation (λ = 0.710 73 Å) for **1** and **9**. Data for **3** were collected at the Advanced Light Source on station 11.3 using a Bruker-AXS ApexII CCD diffractometer with a Silicon 111 monochromator (λ = 0.774 90 Å). The structures were solved by direct methods and refined by full-matrix least-squares on F^2 using the Bruker SHELXTL package. Crystal data of **1**: $C_{12}H_{12}N_2O_3Mo$, fw = 328.18, monoclinic, $P2_1/c$, a = 3.7772(7) Å, b = 15.242(3) Å, c = 20.400(4) Å, β = 95.296(4)° V = 1169.4(4) Å^3, Z = 4, R1 = 0.0412, wR2 = 0.0920 ($I > 2\sigma(I)$), GOF = 1.008. Crystal data of **3**: $C_5H_5NO_3Mo$, fw = 223.04, orthorhombic, $Pbca$, a = 7.5228(4) Å, b = 7.3890(4) Å, c = 22.6080(13) Å, V = 1256.69(12) Å^3, Z = 8, R1 = 0.0501, wR2 = 0.1256 ($I > 2\sigma(I)$), GOF = 1.387. Crystal data of **9**: $C_6H_6NO_3W$, fw = 326.54, tetragonal, $I\bar{4}2m$, a = 5.2546(3) Å, c = 26.987(3) Å, V = 745.14(11) Å^3, Z = 4, R1 = 0.0217, wR2 = 0.0491 ($I > 2\sigma(I)$), GOF = 1.007. These data can be obtained free of charge from The Cambridge Crystallographic Data Centre via www.ccdc.cam.ac.uk/data_ request/cif. The structures were deposited in Cambridge Structural Database (CSD) and the numbers are 952250−952252.

Powder X-ray Diffraction (PXRD). PXRD patterns of all compounds were obtained from a Rigaku D/M-2200T automated diffraction system (Ultima+) with Cu Kα radiation. Measurements were made in a 2θ range 3−50°. The data were collected at room temperature with a step of 0.02° (2θ) and a counting time of 0.2 s/step. The operating power was 40 kV/44 mA.

Data used for the Le Bail refinement and thermal expansion analysis of 1D-WO_3(4,4′-dm-2,2′-bpy) (**2**) and 2D-WO_3(py) (**4**) were collected on Rigaku Ultima IV (Cu Kα radiation) under vacuum in a 2θ range 3−50° (1°/min scan speed, 0.015° step, 2.5° upstream and 5.0° downstream soller slits, 2/3° div slit). Crystal data of **2**: $C_{12}H_{12}N_2O_3W$, fw = 416.09, monoclinic, $P2_1/c$, a = 3.7218(2) Å, b = 15.3615(2) Å, c = 20.3617(8) Å, β = 94.816(6)° V = 1160.03(18) Å^3, Z = 4, R1 = 0.079, wR2 = 0.108 ($I > 2\sigma(I)$). Crystal data of **4**: $C_5H_5NO_3W$ fw = 310.92, orthorhombic, $Pbca$, a = 7.5024(0) Å, b = 7.4283(1) Å, c = 22.9359(2) Å, V = 1278.22(3) Å^3, Z = 8, R1 = 0.131, wR2 = 0.186 ($I > 2\sigma(I)$).

Dielectric Constant Measurements. The cold pressed samples (under 4 T for 4 h) were annealed at different temperature (150 °C for MoO_3(py) and 240 °C for $MoO_3(bpy)_{0.5}$) for 24 h and cooled down to room temperature. The pellets were then covered with silver paint and dried. The free dielectric constant and dielectric loss were measured up to 1 MHz by an impedance analyzer HP4194A.

Thermal Conductivity Measurements. The cold pressed samples (under 3 and 7 mT for 4 h) were annealed 24 h at 250 °C (hybrid samples), 600 °C (MoO_3), and 800 °C (WO_3) before the measurements. The thermal diffusivity and specific heat measurements of the annealed pellet samples were performed in the temperature range 25−105 °C using a laser flash apparatus (Netzsch LFA 457) and differential scanning calorimeter (Netzsch DSC 204 F1), respectively. The thermal conductivity was then calculated using the equation $\kappa(T) = \rho(T)\alpha(T)C_p(T)$, where κ is the thermal conductivity, ρ is the density, α is the diffusivity, and C_p is the specific heat. The thermal conductivity of the idealized "fully-dense" materials was estimated using the effective medium theory.[40]

DFT Calculations. The theoretical calculations were carried out using CASTEP module[41] of a commercial software package (Material Studio 4.4). Generalized gradient approximations (GGA) with Perdew−Burke−Ernzerhof (PBE) exchange-correlation functional (xc) were used in all calculations. Hubbard value of the d orbital of Mo was set to be 2.0 eV. A set of 128, 64, and 32 k-points was used for the calculations of MoO_3, 3D-MoO_3(bpy), and 1D-MoO_3(4,4′-dm-2,2′-bpy), respectively.

RESULTS AND DISCUSSION

By a fine control of synthesis conditions we have succeeded in growing single crystals of a large number of new structures with different dimensionality. Compounds **1** and **2** are infinite 1D chains of a general formula [1D-MO_3(dmbpy) (M = Mo, W) (see Figure 1, Table 1) formed by corner sharing MO_4N_2

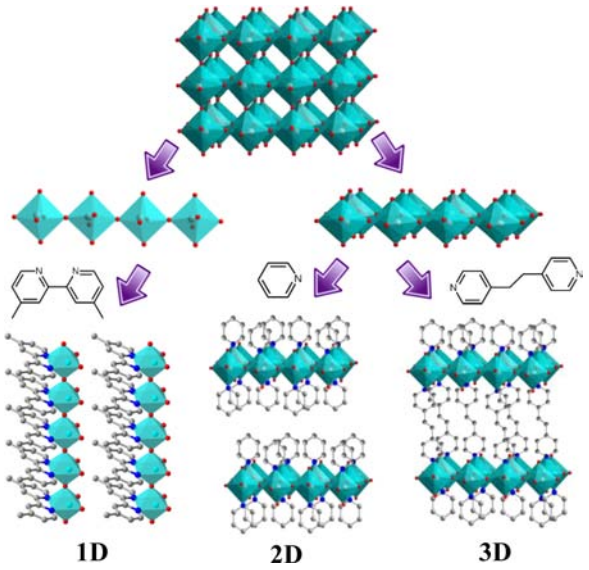

Figure 1. Design and construction of 1D, 2D, and 3D MO_3(L) hybrid semiconductors based on perovskite-like layers of MoO_3 or WO_3 (ReO_3 type structure) and organic linkers: red ball, O; blue ball, N; gray ball, C; light blue ball in the center of octahedron, W or Mo.

connected via dmbpy. Compounds **3** and **4** are 2D networks with a formula of 2D-MO_3(py) (M = Mo, W), where single-atomic MO_3 layers are separated by terminal organic linkers (Figure 1, Table 1). Compounds **5**−**9** are three-dimensional (3D) frameworks with a general formula of [3D-$MO_3(L)_{0.5}$ (M = Mo, W; L = pyz, bpy, bpe). These structures are built on single atomic layers of MO_3 that are interconnected via bridging organic linkers (Figure 1, Table 1). Each MO_3 layer can be considered a "slice" cut from the perovskite-like ReO_3 structure of the parent MO_3 phase. The PXRD analysis indicates that phase-pure samples were obtained in most cases, except compounds **5** and **8**, for which a few very small impurity peaks were found (Supporting Information Figures S1−S2). Thermogravimetric (TG) analysis (see Supporting Information Figures S12−S13) shows that 3D-MoO_3(L) and 3D-WO_3(L) structures are stable up to 300 and 400 °C, respectively. The

dx.doi.org/10.1021/ja4077556 | J. Am. Chem. Soc. 2013, 135, 17401−17407

2D-MO_3(py) structures do not decompose until 180 °C, and the 1D-MO_3(L) structures remain stable at 300 °C. The MO_3 based hybrid semiconductors clearly have significantly higher thermal stability compared to the II−VI hybrid systems.

Selected experimental optical absorption spectra of MoO_3(L) and WO_3(L) hybrid semiconductors, along with their parent MoO_3 and WO_3 compounds, are depicted in Figure 2. Note

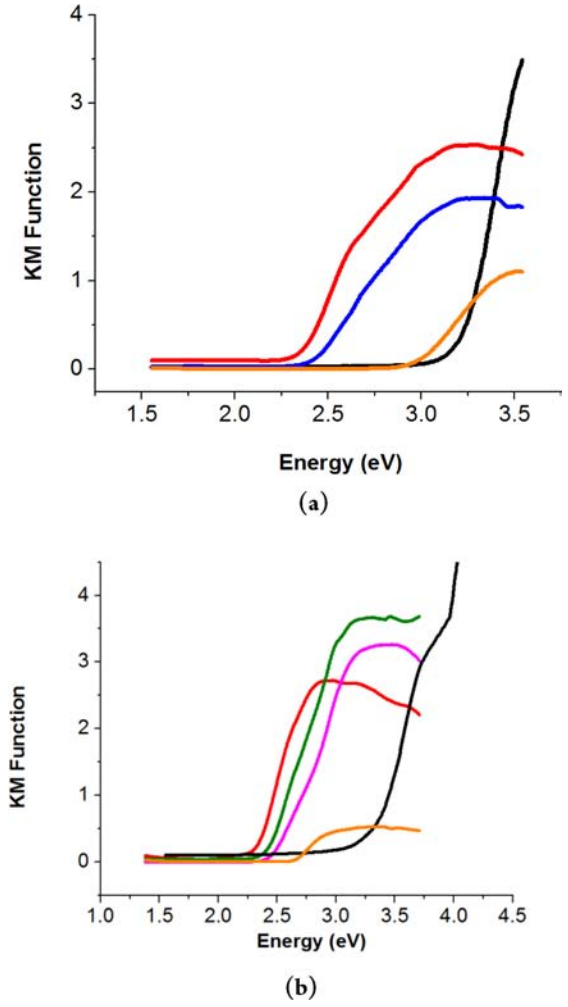

Figure 2. Selected optical absorption spectra of (a) MoO_3(L) (black, **1**; blue, **3**; red, 7) and parent MoO_3 structure (orange); (b) WO_3(L) (black, **2**; pink, **9**; green, **8**; red, **6**) and parent WO_3 structure (orange).

that all MoO_3(L) and WO_3(L) hybrid structures display sharp absorption edge and significantly enhanced absorption intensity compared to their parent compounds MoO_3 and WO_3, indicating that they are much more efficient energy absorbers. It is also interesting to observe the trend of band gap values with respect to the dimensionality, 1D > 2D > 3D (Figure 2), in full accordance with the extent of confinement of the inorganic nanomodules.[16]

Band structure calculations were performed on selected hybrid compounds 1D-MoO_3(4,4′-dm-2,2′-bpy) (**1**) and 3D-MoO_3(4,4′-bpy)$_{0.5}$ (7) and parent structure MoO_3 employing density functional theory (DFT)[41] (Supporting Information Figures S3−S7). Compared to MoO_3 with an indirect band gap of ∼0.5 eV, both **1** and 7 are calculated to be direct band gap semiconductors with band gaps of ∼2.7 and ∼1.7 eV, respectively. The corresponding blue shift values are 2.2 and 1.2 eV for **1** and 7. This phenomenon is very similar to what has been observed in, and well-explained for, the II−VI based hybrid semiconductors, as a consequence of strong structure-induced quantum confinement effect (QCE) when the dimensionality reduces from 3D network to 2D layer and 1D chain, respectively.[8,15,16,20,21] Note that while DFT calculations tend to underestimate the band gaps,[27,42−44] such errors are systematically transformable and can easily be adjusted. For example, the differences between the experimental optical and calculated band gap values are the same for **1** and 7 (both being 0.6 eV, see Table 1 and Supporting Information Figures S3−S4). A similar trend is also found for the WO_3(L) series.

The VI−VI based hybrid semiconductors exhibit greatly enhanced properties compared to their parent structures MoO_3 and WO_3. The estimated thermal conductivity (TC) data of cold pressed pellet samples of 3D-MoO_3(4,4′-bpy)$_{0.5}$ (7) and 3D-WO_3(4,4′-bpy)$_{0.5}$ (**8**) are shown in Figure 3, in comparison

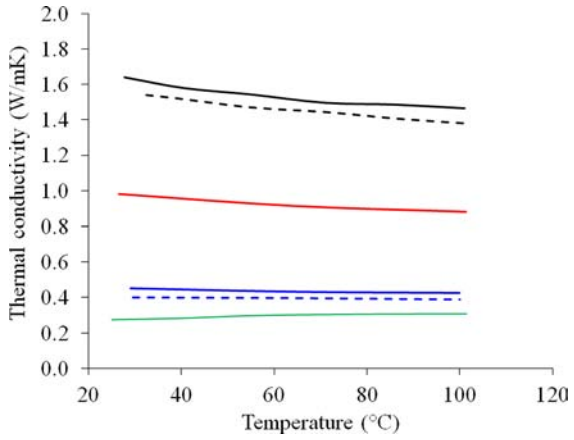

Figure 3. Temperature-dependent thermal conductivities of as-prepared pellet samples of MoO_3 (black), WO_3 (red), 3D-MoO_3(4,4′-bpy)$_{0.5}$ (7, blue), and 3D-WO_3(4,4′-bpy)$_{0.5}$ (**8**, green). The solid lines denote samples cold-pressed at 7 mT, and dotted lines denote samples cold-pressed at 3 mT.

with their parent materials MoO_3 and WO_3. Data on the thermal diffusivity and specific heat of these samples are given in the Supporting Information (Figures S14−15). Compounds 7 and **8** (cold pressed at 7 mT) have a thermal conductivity value of ∼0.44 and 0.28 W/mK at 30 °C, respectively, accounting for a remarkable reduction of 3.5 times from ∼1.54 and 0.98 W/mK for the parent compounds. When the inorganic layers are separated by organic molecules, the interfaces between inorganic layer and organic layer at atomic scale increase phonon scattering substantially. The significance of phonon−interface scattering in the hybrid material is further testified by the temperature insensitivity of their thermal conductivity while the thermal conductivity values of MoO_3 and WO_3 decrease monotonically as the temperature increases over the entire measured range (25−105 °C).

The pressure effect on the sample porosity was evaluated on the MoO_3 and 3D-MoO_3(4,4′-bpy)$_{0.5}$ samples pressed at 3 and 7 t (mT). As shown in Supporting Information Table S3, the sample porosity is very similar for the two pressures. Thus, only slightly higher thermal conductivity values are observed for samples pressed at 7 mT (Figure 3). The small difference in the TC values is possibly due to the small change in the microstructure. As the porous and granular nature of the

dx.doi.org/10.1021/ja4077556 | J. Am. Chem. Soc. 2013, 135, 17401−17407

samples usually lead to lower thermal conductivity than the "ideal" values for fully dense samples, effective medium theory[40] was employed to estimate the thermal conductivity of idealized fully dense samples (see Supporting Information section S11 and Figure S16). The results show that while porosity does reduce the thermal conductivity, such an offset is systematically transformable for all the samples measured. In addition, an overall reduction of TC is calculated to be ~5 and ~3.5 times for the fully dense and as-prepared samples of 3D-MoO_3(4,4′-bpy)$_{0.5}$, respectively (30 °C, 7 mT), suggesting that while porosity effect does play a role, the major contribution comes from the inorganic−organic interface effect of the hybrid materials.

Another interesting property of the VI−VI hybrid semiconductors is their high dielectric constants. Materials with high dielectric constants are being sought as alternative gate dielectrics nanoscale transistors[45,46] and capacitors. Figure 4

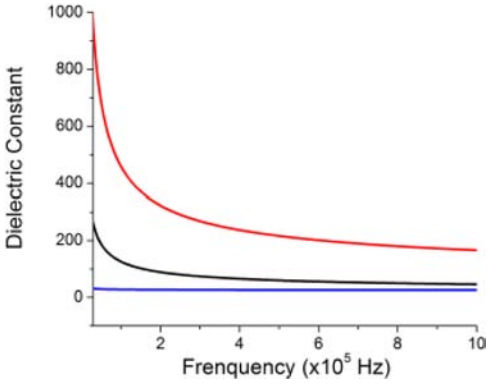

Figure 4. Dielectric constants and of 2D-MoO_3(py) (**3**) (black), 3D-MoO_3(4,4′-bpy)$_{0.5}$ (**7**) (red), and MoO_3 (blue) as a function of frequency (ac electric field).

plots dielectric constants of pellet samples of 2D-MoO_3(py) (**3**) and 3D-MoO_3(4,4′-bpy)$_{0.5}$ (**7**) measured between 10 kHz and 1 MHz using an impedance analyzer (HP4194A). Both compounds have significantly higher values than those of MoO_3. Very high k values are found at low field (e.g., 280 for **3** and 1000 for **7**, respectively, at 20 kHz). The k values decrease dramatically at higher field and reach a constant at ~1 MHz (60 for **3** and 200 for **7** compared to 26 of MoO_3).[47] The high dielectric constants is attributed to the interface-induced space charge polarization in hybrid structures, as the space charges vibrate most strongly at low frequency alternating current (ac) electric field.[48,49] As the interface between electrically conducting and insulating grains is the most important factor for space charge polarization and the hybrid structures are built on two components with distinctly different conductivity, it is not difficult to understand that the inorganic−organic interfaces in these structures are the main reason for space charge polarization, and therefore, high dielectric constants. This is further evidenced as the hybrid structures show higher dielectric losses at low frequencies plotted in Supporting Information Figure S8a, which is caused by the leakage of charges when a large number of space charges accumulate on the structural boundaries. We have also estimated dielectric constants of fully dense MoO_3 and 3D-MoO_3(4,4′-bpy)$_{0.5}$ samples having theoretical density (see Supporting Information Figure S8b). In both cases, higher values are found with respect to those of the pellet samples (with 65.5% and 80.5% of theoretical density values, respectively). The results are not surprising as dielectric constant decreases with decreasing density.

Most materials show positive thermal expansion (PTE) as they expand upon heating. Very few materials show negative thermal expansion (NTE) in which case they contract upon heating.[50,51] Materials exhibiting zero (or nearly zero) thermal expansion (ZTE) behavior are free from thermal shock on rapid heating or cooling.[52,53] Typically they are obtained by combining those of NTE and PTE type. The MO_3 (M = Mo, W) based hybrid structures exhibit interesting negative thermal expansion (NTE) behavior. Powder X-ray diffraction patterns of 3D-MoO_3(4,4′-bpy)$_{0.5}$ (**7**) were collected at various temperatures between 28 and 265 °C. Their structures were solved and refined employing Rietveld refinement method (see Supporting Information Figures S9−S10).[54] The temperature dependent lattice parameters are plotted in Figure 5. The

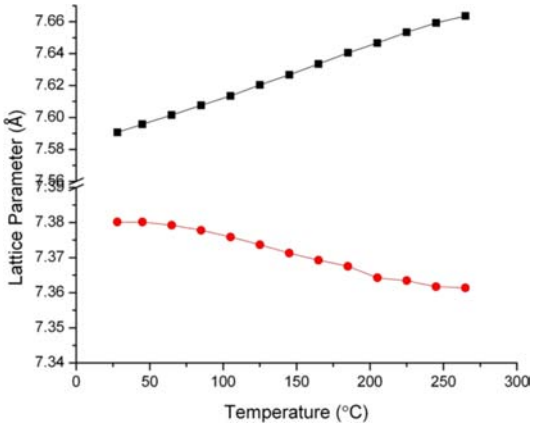

Figure 5. Temperature dependent lattice parameters of the 3D-MoO_3(4,4′-bpy)$_{0.5}$ (**7**) structure shown for a-axis (black) and b-axis (red).

results show a strong negative thermal expansion along the crystallographic b-axis over the entire temperature range. The thermal expansion coefficient is as large as -1.5×10^{-5} K^{-1}, among the highest NTE values reported to date [e.g., α-ZrW_2O_8 (20−430 K), -8.7×10^{-6} K^{-1}; β-ZrW_2O_8 (430−950 K), -4.9×10^{-6} K^{-1}; and γ-ZrW_2O_8 (20−300 K), -1.0×10^{-6} K^{-1}].[55] Unlike the NTE observed in the II−VI hybrid structures which is perpendicular to the inorganic layers (along the layer packing axis),[23,24] the NTE in compound **7** lies within the MoO_3 inorganic layer. A careful view of the crystal structure of **7** at different temperatures reveals that the NTE is caused by changes in the structure, in particular two bond angles. As shown in Supporting Information Figure S11, when temperature is increased from 28 to 265 °C, both Mo2−O6−Mo2 and Mo1−O1−Mo1 angles between the adjacent MoO_5N octahedra decrease significantly from 161.1° to 129.5° and from 137.2° to 132.3°, respectively, resulting in the contraction along the b-axis.

CONCLUSION

In summary, we have designed and constructed a new class of crystalline inorganic−organic hybrid semiconductors built on 1D and 2D MO_3 (or VI−VI) perovskite-like nanomodules and organic linkers. By controlling the dimensionality and topology of the inorganic component and deliberate selection of the organic molecules, we have succeeded in synthesizing a large

dx.doi.org/10.1021/ja4077556 | J. Am. Chem. Soc. 2013, 135, 17401−17407

number of new structures with not only tunable band gaps but also significantly improved properties and new functionality. These include largely reduced thermal conductivity, greatly enhanced dielectric constant, and negative thermal expansion. These interesting and important properties show that the blending of inorganic and organic modules within a crystal lattice is a unique and promising approach in developing multifunctional materials for advanced technological applications.

■ ASSOCIATED CONTENT

Supporting Information

Experimental details, crystallographic data and atomic positions of new structures, powder XRD patterns of all compounds, Rietveld refinement results, TG profiles, DFT calculation results, and estimated thermal conductivity of fully dense samples. This material is available free of charge via the Internet at http://pubs.acs.org.

■ AUTHOR INFORMATION

Corresponding Author

Jingli@rutgers.edu

Notes

The authors declare no competing financial interest.

■ ACKNOWLEDGMENTS

Financial support from the National Science Foundation (Grant DMR-1206700) is gratefully acknowledged. The work on temperature dependent structure analysis at Stony Brook was supported by the U.S. Department of Energy, Office of Science, Office of Basic Energy Sciences under Contract DE-FG02-09ER46650. The Advanced Light Source is supported by the Director, Office of Science, Office of Basic Energy Sciences, of the U.S. Department of Energy under Contract DE-AC02-05CH11231.

■ REFERENCES

(1) Mitzi, D. B. *Adv. Mater.* **2009**, *21*, 3141.
(2) Kagan, C. R.; Mitzi, D. B.; Dimitrakopoulos, C. D. *Science* **1999**, *286*, 945.
(3) Buhro, W. E.; Colvin, V. L. *Nat. Mater.* **2003**, *2*, 138.
(4) Kirchoff, B. K. *Int. J. Plant Sci.* **2003**, *164*, 505.
(5) Era, M.; Morimoto, S.; Tsutsui, T.; Saito, S. *Appl. Phys. Lett.* **1994**, *65*, 676.
(6) Johnson, J. W.; Jacobson, A. J.; Rich, S. M.; Brody, J. F. *J. Am. Chem. Soc.* **1981**, *103*, 5246.
(7) Liu, Y. H.; Porter, S. H.; Goldberger, J. E. *J. Am. Chem. Soc.* **2012**, *134*, 5044.
(8) Huang, X. Y.; Li, J.; Fu, H. X. *J. Am. Chem. Soc.* **2000**, *122*, 8789.
(9) Zhang, Q. C.; Bu, X. H.; Lin, Z.; Wu, T.; Feng, P. Y. *Inorg. Chem.* **2008**, *47*, 9724.
(10) Wu, T.; Bu, X. H.; Liao, P. H.; Wang, L.; Zheng, S. T.; Ma, R.; Feng, P. Y. *J. Am. Chem. Soc.* **2012**, *134*, 3619.
(11) Ingham, B.; Chong, S. V.; Tallon, J. L. *J. Phys. Chem. B* **2005**, *109*, 4936.
(12) Chen, D. L.; Wen, H. J.; Chen, H. M.; Wang, H. L.; Zhang, R.; Xu, H. L.; Yang, D. Y.; Lu, H. X. *Mater. Chem. Phys.* **2009**, *116*, 507.
(13) Gauthron, K.; Lauret, J. S.; Doyennette, L.; Lanty, G.; Al Choueiry, A.; Zhang, S. J.; Brehier, A.; Largeau, L.; Mauguin, O.; Bloch, J.; Deleporte, E. *Opt. Express* **2010**, *18*, 5912.
(14) Wu, M.; Rhee, J.; Emge, T. J.; Yao, H. B.; Cheng, J. H.; Thiagarajan, S.; Croft, M.; Yang, R. G.; Li, J. *Chem. Commun.* **2010**, *46*, 1649.
(15) Huang, X. Y.; Li, J.; Zhang, Y.; Mascarenhas, A. *J. Am. Chem. Soc.* **2003**, *125*, 7049.
(16) Huang, X. Y.; Li, J. *J. Am. Chem. Soc.* **2007**, *129*, 3157.
(17) Huang, X. Y.; Roushan, M.; Emge, T. J.; Bi, W. H.; Thiagarajan, S.; Cheng, J. H.; Yang, R. G.; Li, J. *Angew. Chem., Int. Ed.* **2009**, *48*, 7871.
(18) Yao, H. B.; Zhang, X. A.; Wang, X. H.; Yu, S. H.; Li, J. *Dalton Trans.* **2011**, *40*, 3191.
(19) Ouyang, X.; Tsai, T. Y.; Chen, D. H.; Huang, Q. J.; Cheng, W. H.; Clearfield, A. *Chem. Commun.* **2003**, 1107.
(20) Fluegel, B.; Zhang, Y.; Mascarenhas, A.; Huang, X.; Li, J. *Phys. Rev. B* **2004**, *70*, 205308.
(21) Fu, H. X.; Li, J. *J. Chem. Phys.* **2004**, *120*, 6721.
(22) Zhang, Y.; Dalpian, G. M.; Fluegel, B.; Wei, S. H.; Mascarenhas, A.; Huang, X. Y.; Li, J.; Wang, L. W. *Phys. Rev. Lett.* **2006**, 96.
(23) Li, J.; Bi, W. H.; Ki, W.; Huang, X. Y.; Reddy, S. *J. Am. Chem. Soc.* **2007**, *129*, 14140.
(24) Zhang, Y.; Islam, Z.; Ren, Y.; Parilla, P. A.; Ahrenkiel, S. P.; Lee, P. L.; Mascarenhas, A.; McNevin, M. J.; Naumov, I.; Fu, H. X.; Huang, X. Y.; Li, J. *Phys. Rev. Lett.* **2007**, *99*, 215901.
(25) Ki, W.; Li, J. *J. Am. Chem. Soc.* **2008**, *130*, 8114.
(26) Roushan, M.; Zhang, X.; Li, J. *Angew. Chem., Int. Ed.* **2012**, *51*, 436.
(27) Zhang, R. B.; Emge, T. J.; Zheng, C.; Li, J. *J. Mater. Chem. A* **2013**, *1*, 199.
(28) Yao, W. T.; Yu, S. H.; Huang, X. Y.; Jiang, J.; Zhao, L. Q.; Pan, L.; Li, J. *Adv. Mater.* **2005**, *17*, 2799.
(29) Chernova, N. A.; Roppolo, M.; Dillon, A. C.; Whittingham, M. S. *J. Mater. Chem.* **2009**, *19*, 2526.
(30) Zheng, H. D.; Ou, J. Z.; Strano, M. S.; Kaner, R. B.; Mitchell, A.; Kalantar-Zadeh, K. *Adv. Funct. Mater.* **2011**, *21*, 2175.
(31) Gratzel, M. *Nature* **2001**, *414*, 338.
(32) Santato, C.; Ulmann, M.; Augustynski, J. *J. Phys. Chem. B* **2001**, *105*, 936.
(33) Zheng, H. D.; Tachibana, Y.; Kalantar-zadeh, K. *Langmuir* **2010**, *26*, 19148.
(34) Lee, S. H.; Deshpande, R.; Parilla, P. A.; Jones, K. M.; To, B.; Mahan, A. H.; Dillon, A. C. *Adv. Mater.* **2006**, *18*, 763.
(35) Lee, S. H.; Kim, Y. H.; Deshpande, R.; Parilla, P. A.; Whitney, E.; Gillaspie, D. T.; Jones, K. M.; Mahan, A. H.; Zhang, S. B.; Dillon, A. C. *Adv. Mater.* **2008**, *20*, 3627.
(36) Anilkumar, K. R.; Parveen, A.; Badiger, G. R.; Prasad, M. V. N. A. *Ferroelectrics* **2009**, *386*, 88.
(37) Xu, Y.; Lu, J. J.; Goh, N. K. *J. Mater. Chem.* **1999**, *9*, 1599.
(38) Yan, B. B.; Xu, Y.; Goh, N. K.; Chia, L. S. *Chem. Commun.* **2000**, 2169.
(39) Hagrman, P. J.; LaDuca, R. L.; Koo, H. J.; Rarig, R.; Haushalter, R. C.; Whangbo, M. H.; Zubieta, J. *Inorg. Chem.* **2000**, *39*, 4311.
(40) Wan, M. P. N. *Mater. Sci. Eng., R* **2008**, *63*, 1.
(41) Clark, S. J.; Segall, M. D.; Pickard, C. J.; Hasnip, P. J.; Probert, M. J.; Refson, K.; Payne, M. C. *Z. Kristallogr.* **2005**, *220*, 567.
(42) Delerue, C.; Lannoo, M.; Allan, G. *Phys. Rev. Lett.* **2000**, *84*, 2457.
(43) Sham, L. J.; Schluter, M. *Phys. Rev. Lett.* **1983**, *51*, 1888.
(44) Perdew, J. P.; Parr, R. G.; Levy, M.; Balduz, J. L., Jr. *Phys. Rev. Lett.* **1982**, *49*, 1691.
(45) Robertson, J. *Rep. Prog. Phys.* **2006**, *69*, 327.
(46) Wang, L.; Yoon, M. H.; Lu, G.; Yang, Y.; Facchetti, A.; Marks, T. J. *Nat. Mater.* **2006**, *5*, 893.
(47) Sayer, M.; Mansingh, A.; Webb, T. B.; Noad, J. J. P. C. *J. Phys. Chem.* **1978**, *11*, 315.
(48) Zhang, X. G.; Pantelides, S. T. *Phys. Rev. Lett.* **2012**, *108*, 266602.
(49) *Polar Oxides—Properties, Characterization, and Imaging*; Waser, R., Böttger, U., Tiedke, S., Eds.; WILEY-VCH Verlag GmbH & Co.: New York, 2005.
(50) Greve, B. K.; Martin, K. L.; Lee, P. L.; Chupas, P. J.; Chapman, K. W.; Wilkinson, A. P. *J. Am. Chem. Soc.* **2010**, *132*, 15496.
(51) Mary, T. A.; Evans, J. S. O.; Vogt, T.; Sleight, A. W. *Science* **1996**, *272*, 90.

(52) Zhang, X.; Ren, Y.; Roushan, M.; Li, J. *Eur. J. Inorg. Chem.* **2012**, 5966.
(53) Salvador, J. R.; Gu, F.; Hogan, T.; Kanatzidis, M. G. *Nature* **2003**, *425*, 702.
(54) Rietveld, H. M. *J. Appl. Crystallogr.* **1969**, *2*, 65.
(55) Sleight, A. W. *Annu. Rev. Mater. Sci.* **1998**, *28*, 29.